Hindawi
Advances in Civil Engineering
Volume 2021, Article ID 6627959, 9 pages
https://doi.org/10.1155/2021/6627959

*Research Article*

# Energy Dissipation and Damage Evolution Characteristics of Salt Rock under Uniaxial Cyclic Loading and Unloading Tension

**Anqi Zhu,[1] Jianfeng Liu,[1] Zhide Wu,[2] Lu Wang,[1] Hejuan Liu,[3] Fukun Xiao,[4] and Chaofu Deng[5]**

[1]*State Key Laboratory of Hydraulic and Mountain River Engineering, Sichuan University, Chengdu 610065, China*
[2]*CNPC Key Laboratory of Oil and Gas Underground Storage Engineering, Langfang 065007, China*
[3]*Institute of Rock and Soil Mechanics, Chinese Academy of Sciences, State Key Experiments in Geotechnical Mechanics and Engineering, Wuhan 430071, China*
[4]*Heilongjiang Ground Pressure and Gas Control in Deep Mining Key Laboratory, Heilongjiang University of Science and Technology, Harbin, Heilongjiang 150022, China*
[5]*Comprehensive Section of National Economy, Panzhihua Development and Reform Commission, Panzhihua, Sichuan 617000, China*

Correspondence should be addressed to Jianfeng Liu; liujf@scu.edu.cn

Received 12 October 2020; Revised 4 April 2021; Accepted 9 April 2021; Published 20 May 2021

Academic Editor: Daniele Baraldi



Salt rock has been regarded as the optimal surrounding rock for underground gas storage (UGS), and it is occasionally subjected to cyclic tension because of the gas injection and production of salt cavern, which leads to the change in mechanical properties of salt rock. In this paper, a laboratory study is conducted to investigate the energy dissipation and damage evolution characteristics of salt rock under uniaxial cyclic tension monitored by acoustic emission (AE) machine. Compared to monotonic tension, both tensile strength and deformation capacity of salt rock are enhanced under cyclic tension. The fracture crack is approximately a single linear crack with large elliptical plastic deformation zone, which is consistent with the spatial distribution of AE events. In yield stage, the proportion of dissipative energy increases first but decreases subsequently. The relationship between AE energy-based damage variable and displacement is established. It is concluded that the damage variable is a piecewise power correlation with displacement while the growth rate of damage variable increases in the pre-peak stage but decreases in post-peak stage.

## 1. Introduction

Underground energy storage is an economical and advanced method for the storage of critical energy like natural gas, hydrogen, compressed air, and oil [1, 2]. However, because of the gas injection and production of salt cavern, the surrounding salt rock was gradually damaged by the disturbance of external load [3, 4]. The surrounding rock in a underground cavern is subjected to cyclic excavation-induced stress, which leads to notable changes in the mechanical properties [5–7]. Therefore, it is of great importance to study the mechanical properties and damage evolution characteristics of salt rock under uniaxial cyclic tension.

In recent years, due to the increasing attention to underground salt cavern, various experiments on salt rock have been conducted. In most cases, the study on salt rock mainly focuses on quantifying the compressive strength, deformation capacity, creep behaviour, and self-healing capacity to provide practical data for the design and long-term operation safety evaluation of salt cavern [8–10]. However, considering that rock is vulnerable under tensile stress, tensile strength of rock should be deeply studied. A series of tension tests, including direct tension test and Brazilian test, had been conducted by researchers [11–13] and found that the tensile strength is approximately at 0.846 MPa, which is very low compared to granite, sandstone, and marble. Besides, they also proposed the differences in tensile strength and failure characteristics under different experimental methods. However, the aforementioned experimental researches scarcely involve a deep analysis on the damage

evolution of salt rock under the tension especially cyclic tension tests, considering that surrounding rock of salt cavern is subjected to regular gas injection and production.

During the cyclic tension test, the energy input by external work is partly converted into elastic strain energy and stored in rock, and the rest is transformed into dissipative energy [14–16]. Xie et al. [17] found that the deformation and failure process of rocks is controlled by energy dissipation. This conclusion was proved by many experimental results and became an important method to study the rock deformation and failure. The energy evolution characteristics of different rocks under different loading paths were investigated by researchers, and they proposed that the proportion of dissipative energy could predict the failure of rock. The abrupt increase in the proportion of dissipative energy usually depicts the fracture of rocks [18]. Moreover, AE energy method was also employed to estimate the deformation and failure of rock. Parameters like AE count and energy could represent the damage evolution characteristics of rock during deformation [19–22]. The researchers deeply investigated the relationship between rock deformation and AE events and concluded that the AE energy evolution could reflect the damage evolution of limestone [23]. The combined use of AE energy and strain energy could be an efficient way to study the damage evolution in salt rock under uniaxial cyclic tension.

Generally, uniaxial compression or tensile tests on rock material like granite, sandstone, and salt rock were performed. However, in the process of underground excavation, the surrounding rock is mostly subjected to cyclic load which may cause different results. Therefore, to understand the energy and damage evolution characteristics of salt rock, both monotonic loading and cyclic loading tension tests on salt disc were conducted. An AE device was also employed to estimate the crack propagation and damage evolution of rock specimen. Then, effects of cyclic tension on the mechanical properties, energy dissipation, and damage evolution characteristics were discussed. A piecewise power function was proposed to describe the relationship between AE energy-based damage variable and displacement of salt rock under cyclic tension.

## 2. Experiments

*2.1. Specimen Preparation.* Raw salt rock samples were processed into standard Brazilian discs following the standard recommended by Chinese Society of Rock Mechanics [24], with the height of 45 mm and the diameter of 90 mm (Figure 1). The average density of salt rock specimen was 2.17 g/cm$^3$, and the salt rock was mainly composed of 95~99% NaCl, 1~5% $CaSO_4$, ~0.3% $Fe_2O_3$.

*2.2. Testing Apparatus.* Laboratory tests on salt rock were conducted on the MTS.815 rock mechanics test system. The testing system is composed of an AE machine, a central control computer, a wave velocity test equipment, and a loading machine, which is capable of applying a maximum axial load of 4600 kN (Figure 2). A pair of Linear Variable


Figure 1: Salt rock specimen.

Differential Transformers (LVDT) were installed symmetrically on the test platform, and the measuring range of axial deformation is from −2.5 mm to 2.5 mm. The measurement and control precision of all devices is 0.5%. In order to estimate the damage evolution in salt rock specimen during the test, a PCI-II acoustic emission (AE) system, which consists of an AE recording and analyzing machine, amplifiers, and AE sensors, was adopted (Figure 2). The AE system can monitor the crack growth in salt rock in real time. In order to obtain the three-dimensional time-space location map of acoustic emission events in rock, eight AE sensors were installed on the specimen as shown in Figure 2, and the type of AE sensors is $R3\alpha$ of which the detecting frequency ranges within 20~180 Hz. They were installed symmetrically using two elastic fixtures with the distance to the longitudinal axis measured at 20 mm and the distance to the interface measured at 20 mm (Figure 2(c)). Also, to enhance the AE signal, the contact surface between the AE sensors and the disc is applied with Vaseline. The gain of the amplifiers is 40 dB, and the threshold is 35 dB. According to the Brazilian test standard proposed by CSRM, the tensile strength of rock can be calculated as follows [24]:

$$\sigma_t = \frac{2P_t}{\pi\, DL}, \tag{1}$$

where $\sigma_t$ stands for tensile strength of rock (Pa), $P_t$ is the maximum load (N), $D$ stands for the diameter of Brazilian rock specimen (m), and $L$ represents the height of Brazilian disc specimen (m).

*2.3. Test Procedure.* According to the tension test results of salt rock conducted in our laboratory, the average tensile strength of salt rock features is 1.07 MPa (Table 1). For monotonic loading test, the LVDT was employed to control the tensile rate at 0.3 mm/min in the whole loading process. For cyclic loading test, the loading procedure was the same as monotonic loading while the unloading started when the maximum axial force increased by 0.5 kN. However, in the pre-peak stage, manual control mode was adopted for the cyclic loading process, and the loading procedure was the same as monotonic loading while the unloading started when axial stress reaches the peak in this cycle. The lower unloading limit of every cycle was 0.3 kN. Moreover, all tests were conducted under the premise of accurate AE locations, and the errors of AE location were eliminated by knocking at different spots on the specimen before each tension test.

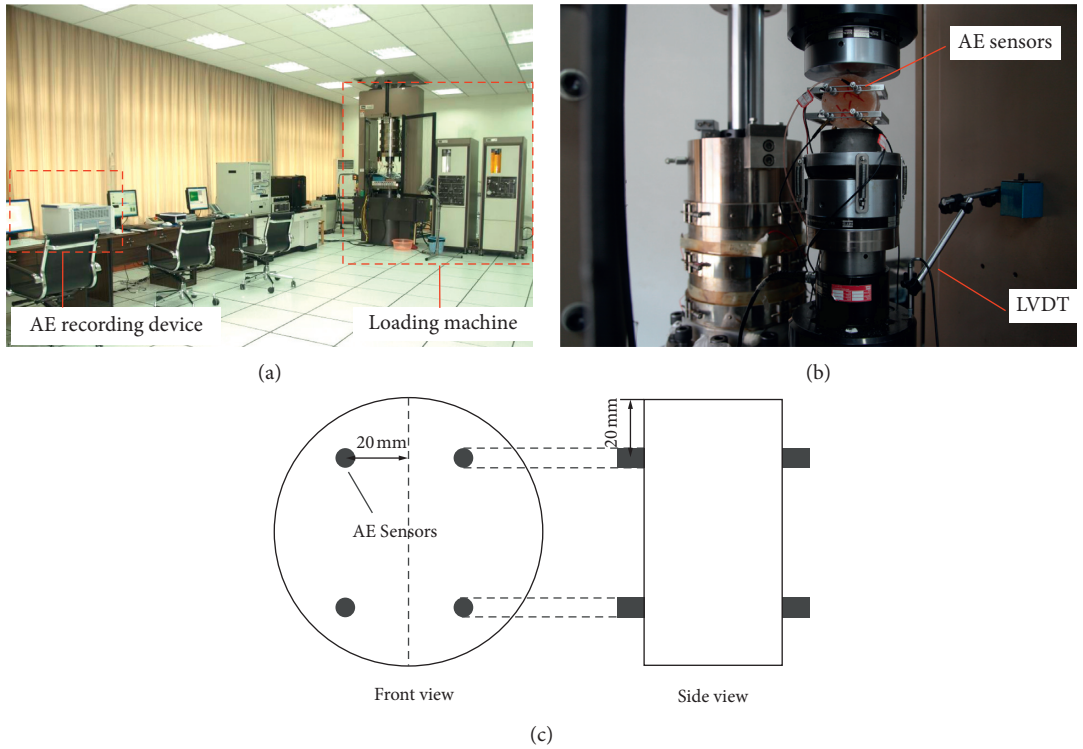


Figure 2: Testing apparatus. (a) MTS.815 rock mechanics test system. (b) Brazilian test with AE monitoring. (c) Layout coordinate diagram of AE sensors and LVDTs.

Table 1: Mechanical parameters of salt rock under monotonic loading and cyclic tension.

| Specimen | | Maximum load $P_t$/kN | Tensile strength $\sigma_t$/MPa | Axial displacement $\Delta l$/mm |
|---|---|---|---|---|
| Monotonic loading | d-1 | 6.10 | 0.96 | 0.74 |
| | d-2 | 7.69 | 1.21 | 0.86 |
| | d-3 | 6.57 | 1.03 | 0.82 |
| | Average | 6.79 | 1.07 | 0.81 |
| Cyclic tension | f-1 | 6.76 | 1.06 | 1.50 |
| | f-2 | 9.52 | 1.50 | 1.59 |
| | f-3 | 6.38 | 1.00 | 1.73 |
| | Average | 7.55 | 1.19 | 1.60 |

## 3. Experimental Results

*3.1. Mechanical Properties.* Both monotonic loading and cyclic Brazilian splitting tests were conducted, and basic mechanical parameters obtained through the tests are shown in Figure 3. The average tensile strengths of salt rock under different loading paths are close, with the figure of 1.07 MPa for monotonic loading and 1.19 MPa for cyclic, respectively. You [25] and Zhao [26] pointed out that the microcracks inside rock were more closed due to the cyclic loading, which consequently enhanced the frictional strength and caused an increase in the rock strength, compared to monotonic loading. Notably, there is a considerable increase in the axial displacement at the peak strength point. The average axial displacement for monotonic loading is 0.81 mm, while the figure for cyclic tension increases by 97.63%, which indicates that the deformation capacity of salt rock is significantly enhanced.

Typical stress-displacement curves of salt rock specimen under different loading paths are plotted in Figure 3. A short elastic stage is observed on both curves, which indicates that the tensile yield strength of salt rock is slightly below 0.2 MPa. In the process of loading, when the stress exceeds the previous unloading load, the stress-strain curve will rise along the original loading curve like the monotonic loading. This phenomenon is called the deformation memory phenomenon of rock, and the unloading modulus of rock can be obtained based on it.

*3.2. AE Counts and Energy.* Acoustic emission hit count and energy are reliable parameters in estimating the basic damage evolution characteristics in rock. The AE count and energy curves of salt rock specimen f-1 are shown in Figure 4, and the stress-time curve is also plotted.

The average values of AE hit count rate and energy rate in single cycle increase before peak stress and decrease after the

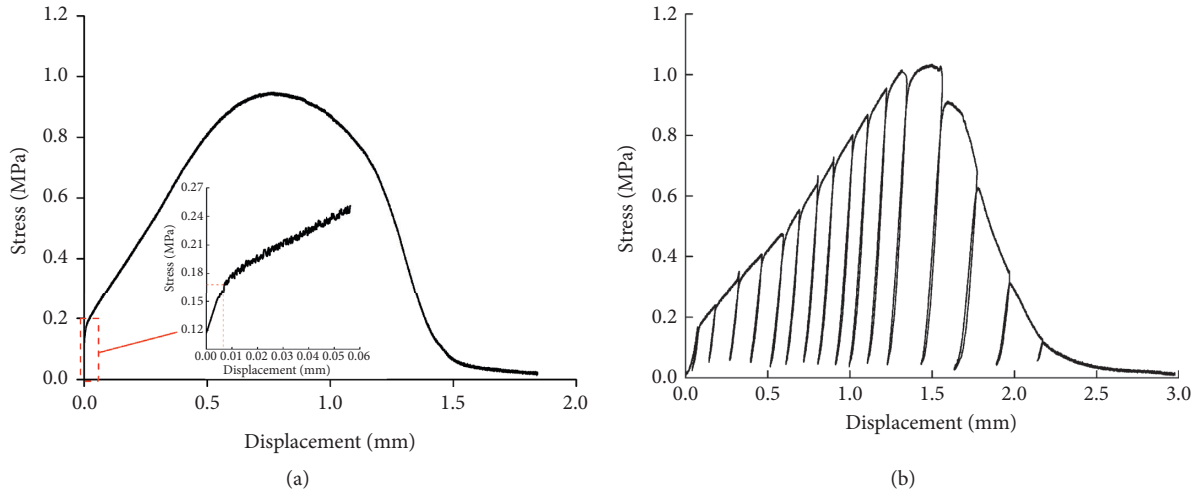


Figure 3: Stress-displacement curves of salt rock specimens. (a) Specimen d-1; (b) specimen f-1.

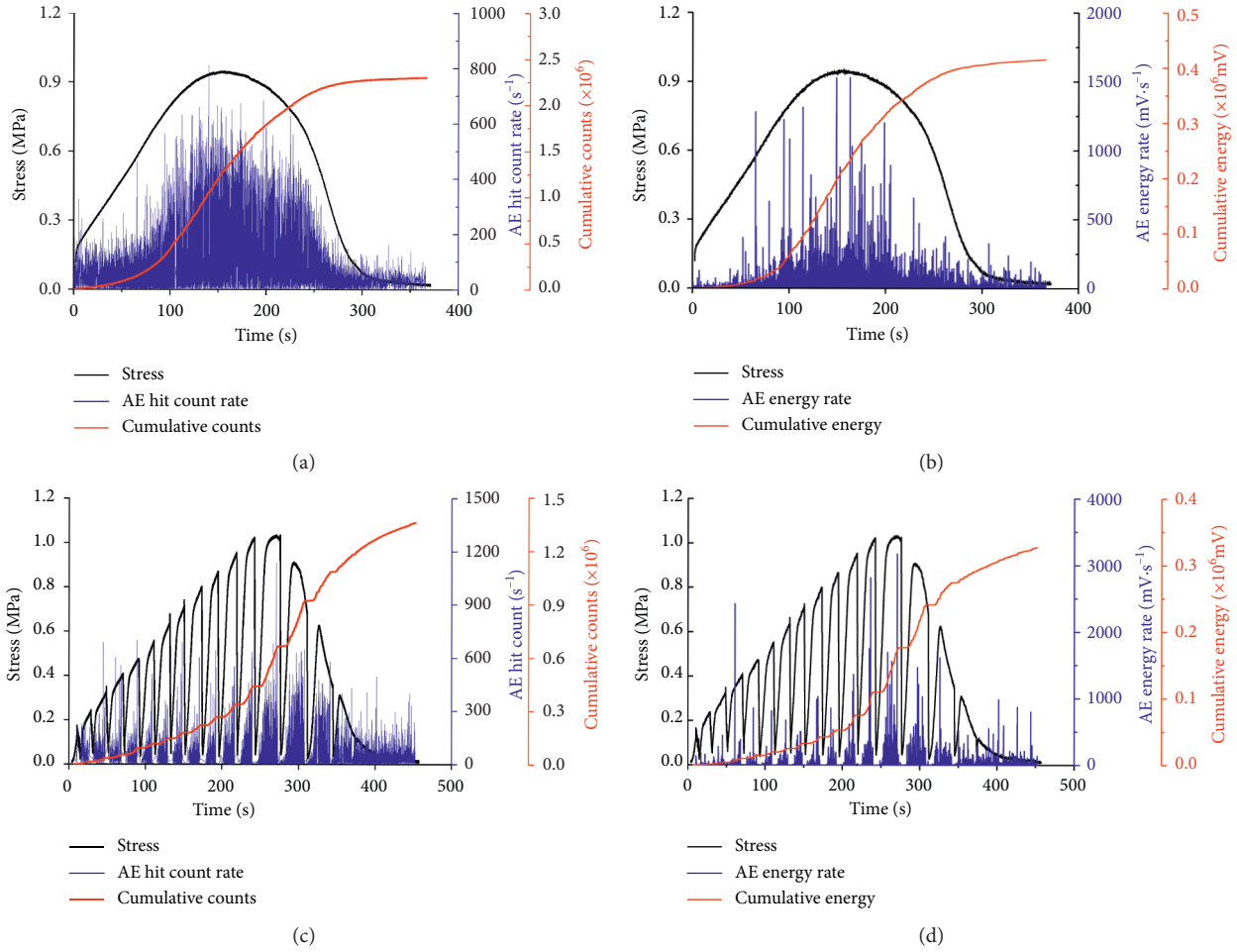


Figure 4: Stress-time, AE characteristic parameters-time curves of salt rock. (a) AE hit count of specimen d-1. (b) AE energy of specimen d-1. (c) AE hit count of specimen f-1. (d) AE energy of specimen d-1.

peak stress. It is also observed that with the envelopes of AE hit count rate and energy rate curves are highly similar with the stress-time curve. At the beginning of loading, the deformation of the specimen is small, and the tensile stress is low; the AE hit count rate and energy rate are at a low level; thus the cumulative hit count and cumulative energy curve are relatively gentle.

It is observed from Figure 4 that the AE hit count rate and energy gradually become active with the increase in

tensile stress and the deformation of specimen. Also, the accumulative hit counts and accumulative energy progressively rise with the increase in tensile stress. It can be seen that the AE signal activity is positively correlated with the specimen stress from the beginning of load application to the peak stress stage. The greater the load is, the more active AE signal is. Notably, the Kaiser effect of rock salt during the process is obvious as shown in Figure 4. In terms of single cycle, the increase of accumulative hit count rate and accumulative energy rate of salt rock gradually increases with the increase in stress. The slope of accumulative hit count rate curve and accumulative energy rate curve increase continuously until the peak stress. AE hit count rate and energy rate reach the maximum value at the peak stress; thus the slope of cumulative energy curve reaches the maximum. After the peak stress, the cumulative hit count and cumulative energy increase to the maximum, and the AE signal intensity reaches the maximum when the stress reaches the peak.

Compared to cyclic tension, AE signals are more active under monotonic tension. The cumulative hit count and cumulative energy under cyclic tension test are $1.36 \times 10^6$ and $0.33 \times 10^6$ mV, respectively, compared to $2.30 \times 10^6$ and $0.41 \times 10^6$ mV, respectively, for monotonic tension test. By contrast, the highest figures of AE hit count and AE energy for monotonic tension test reach $825\ s^{-1}$ and $1592\ mV \cdot s^{-1}$. However, the highest figures of AE hit count and AE energy for cyclic tension test are $1132\ s^{-1}$ and $3289\ mV \cdot s^{-1}$, respectively.

## 4. Discussion

*4.1. AE Time-Space Diagram and Failure Characteristics.* During the monotonic and cyclic tension test, the spatial coordinates and time of all AE events were recorded. Therefore, the spatiotemporal map of AE events could be obtained based on the experimental results. The spatiotemporal maps of AE events of salt rock specimen d-1 and f-1 are plotted in Figure 5 along with the stress-displacement curves and the photos of damaged salt rock specimens after Brazilian test. The spatiotemporal map of AE events of different stages was also plotted to analyze the damage evolution process of salt rock.

According to the AE spatiotemporal map, the deformation and failure of Brazilian disc specimen began from the contact surface of specimen and testing platform and gradually extended to the center of the disc. Eventually, an approximately linear macrocrack formed, and the salt rock specimen was fractured, which was consistent with the failure characteristics of salt rock specimen in Figure 5. Only a few AE events were generated in the elastic stage which concentrated near the upper and lower symmetrical contact surface. With the increase in axial load, microcracks on salt rock specimen gradually extended both horizontally and vertically, and an elliptical plastic deformation zone was formed. After that, the microcracks were gradually connected and the macrocrack came into existence, and the specimen was fractured when the axial stress reached its tensile strength. In the post-peak stage, the macrocrack progressively widened and the plastic deformation zone also expanded. It is noted that there are more cracks on the rock specimen under monotonic loading compared to cyclic loading, which is inconsistent with the AE results which demonstrates that there are more AE events and wider plastic deformation zone on specimen under monotonic loading. For salt rock, the failure modes are transgranular fracture mode and intergranular fracture mode, and the AE signal is stronger for transgranular fracture. According to stress-strain curves in Figure 3, it is observed that the tension strength of salt rock is slightly enhanced by cyclic loading process, thus decreasing the fracture degree of transgranular fracture. According to test results, there are more cracks on the salt rock sample under monotic tension test, compared to the specimen under cyclic tension. It is also noted that though there are throughout cracks on both samples; the crack width on the salt rock under monotic tension is much larger than the other one, which demonstrates that salt rock is less damaged under monotic tension.

*4.2. Energy Dissipation Ratio.* During the deformation and failure process of rock under cyclic tension, the energy input by external force is mainly converted into the elastic energy $U_e$, which was stored in the rock, and the dissipated energy $U_d$ consumed by the rock failure caused by internal damage. Moreover, the elastic energy $U_e$ could be released in the unloading process with the partial recovery of deformation [28]. In addition, the loading lag effect leads to the inconsistency between the unloading point A and the maximum displacement point B in the loading process. After the unloading starts, the rock will still produce small positive deformation under the action of force. At this stage, the machine inputs positive work, so the load displacement curve of single cycle under typical cyclic tension can be obtained (Figure 6).

According to the basic principle, the input energy $U_0$, dissipation energy $U_d$, and elastic energy $U_e$ of salt rock under different cycles are obtained. To investigate the energy evolution characteristics, two parameters are introduced which are defined as the following equations:

$$\begin{cases} k_e = \dfrac{U_e}{U_0}, \\ \\ k_d = \dfrac{U_d}{U_0}, \end{cases} \tag{2}$$

where $k_e$ is proportion of elastic energy in a single cycle and $k_d$ is proportion of dissipative energy in a single cycle. Therefore, these two parameters could describe the basic energy evolution features in the whole process.

As shown in Figure 7, the peak stress in the first cycle is within the elastic stage of salt rock, and the proportion of dissipative energy is relatively low, which indicates that most input energy was transformed into elastic energy which was released in unloading process in the first cycle. However, with the increase in the axial load, there is a significant

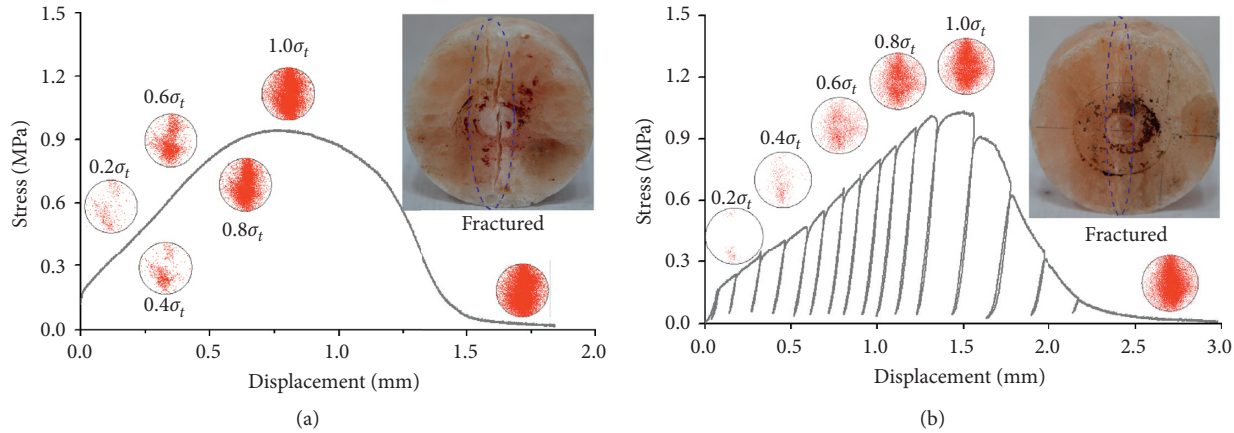


Figure 5: Spatiotemporal map of AE events of different stages and fractured salt rock specimens. (a) d-1; (b) f-1.

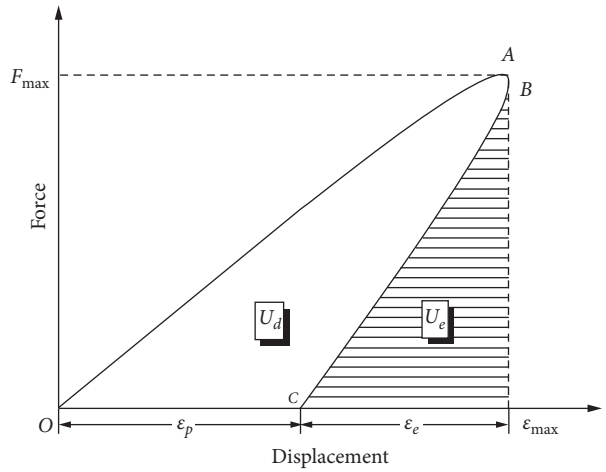


Figure 6: Energy dissipation characteristics of single.

increase in the proportion of dissipative energy, from approximately 0.51 to 0.80. In the yield stage, the proportion of dissipative energy decreases first and then increases, making it approximately a *U*-shape curve. Combined with the aforementioned experimental results from the stress-displacement curves, we can infer that the cyclic loading and unloading enhance elastic energy storage capacity of salt rock at low level stress but gradually deteriorate with the promotion of stress. Since salt rock is soft, the specimens are fractured after reaching the tensile strength. However, a notable increase in dissipative energy also occurs when reaching the peak strength of salt rock, and the proportion of dissipative energy rises rapidly in the post-peak stage, which indicates that salt rock is greatly damaged in the cycle which reaches peak strength.

*4.3. Damage Evolution Characteristics.* Influenced by the deposition, water movement, geological tectonic movement, and sampling, there are many randomly distributed pores in the rock samples. Based on continuum theory, a constitutive equation of rock strength considering damage variable was established by Tang et al. [27]:

$$\sigma = E\varepsilon(1 - D_a), \tag{3}$$

where $\sigma$ stands for the strength of damaged rock, $E$ represents the elastic modulus of rock, $\varepsilon$ is the strain, and $D_a$ stands for damage variable. The damage variable can be calculated based on the AE energy results as follows:

$$D_a = \frac{N(\sigma_t)}{N_0}, \tag{4}$$

where $N(\sigma_t)$ is the accumulative AE energy when the axial stress reaches $\sigma_t$ and $N_0$ is the accumulative AE energy when the test is finished. Therefore, the damage variable-strain curves are plotted in Figure 8 to demonstrate the damage evolution characteristics of salt rock under uniaxial cyclic tension. The damage variable-strain curves of three salt rock specimens show the same changing laws, which indicates that the damage in salt rock increases with increasing rock deformation.

Based on the aforementioned features of the damage variable-displacement curves, the damage variable-displacement curves were divided into two sections, taking the peak stress point as the boundary, and we then fitted each section using different functions. The fitting results in the pre-peak and post-peak stage are shown in Figure 9; the relationships between damage variable and displacement can be expressed as power function with different parameters:

$$D_a = \begin{cases} ml^n, & l \le l, \\ a(l-b)c, & l > l_t, \end{cases} \tag{5}$$

where $l$ is the displacement(mm), $l_t$ is displacement of salt rock at tensile peak strength, and $m, n, a, b, c$ are the fitting parameters. The fitting results can represent the damage variable evolution characteristics during the test with the square of regression coefficients for all sections higher than 0.90. The fitting results demonstrated that while the damage in salt rock increases with increasing rock deformation, the derivatives of the functions increase first but decrease later, indicating the growth rate of damage variable changes after reaching rock tensile strength. The growth rate of damage variable progressively increases in the pre-peak stage while gradually decreases in the post-peak stage [28].

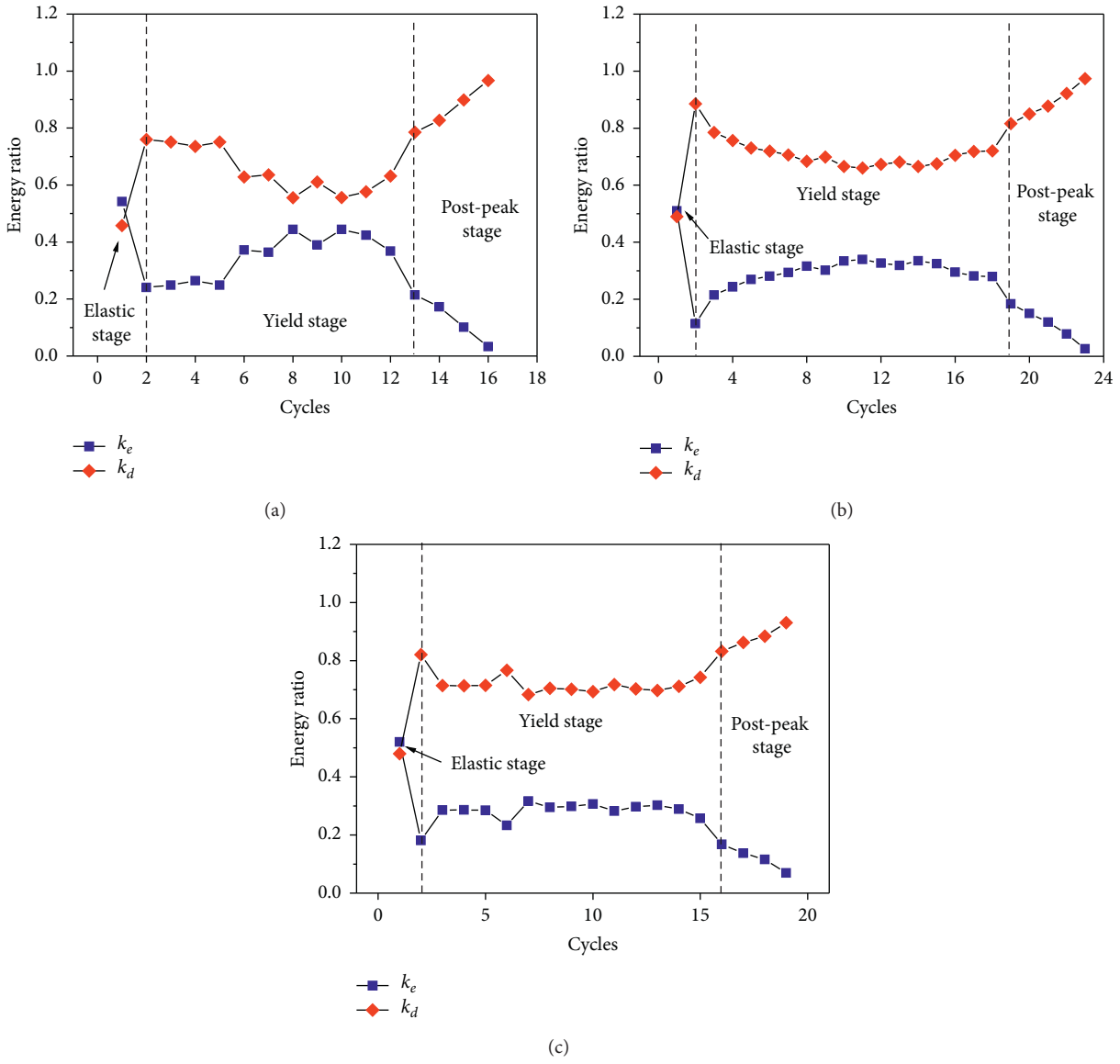


Figure 7: Evolution characteristics of proportion of elastic and dissipative energy. (a) f-1; (b) f-2; (c) f-3.

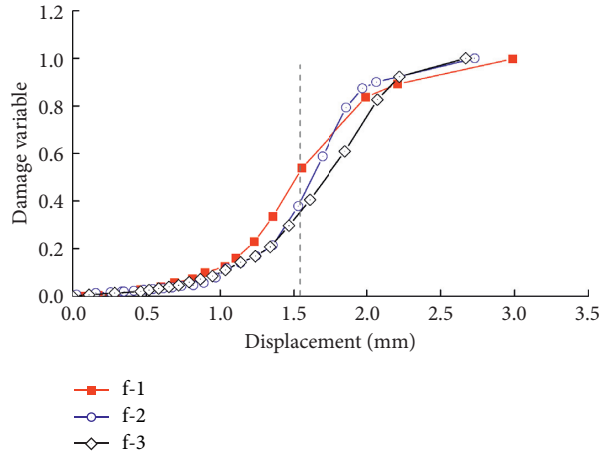


Figure 8: The damage variable-displacement curves of salt rock specimens.

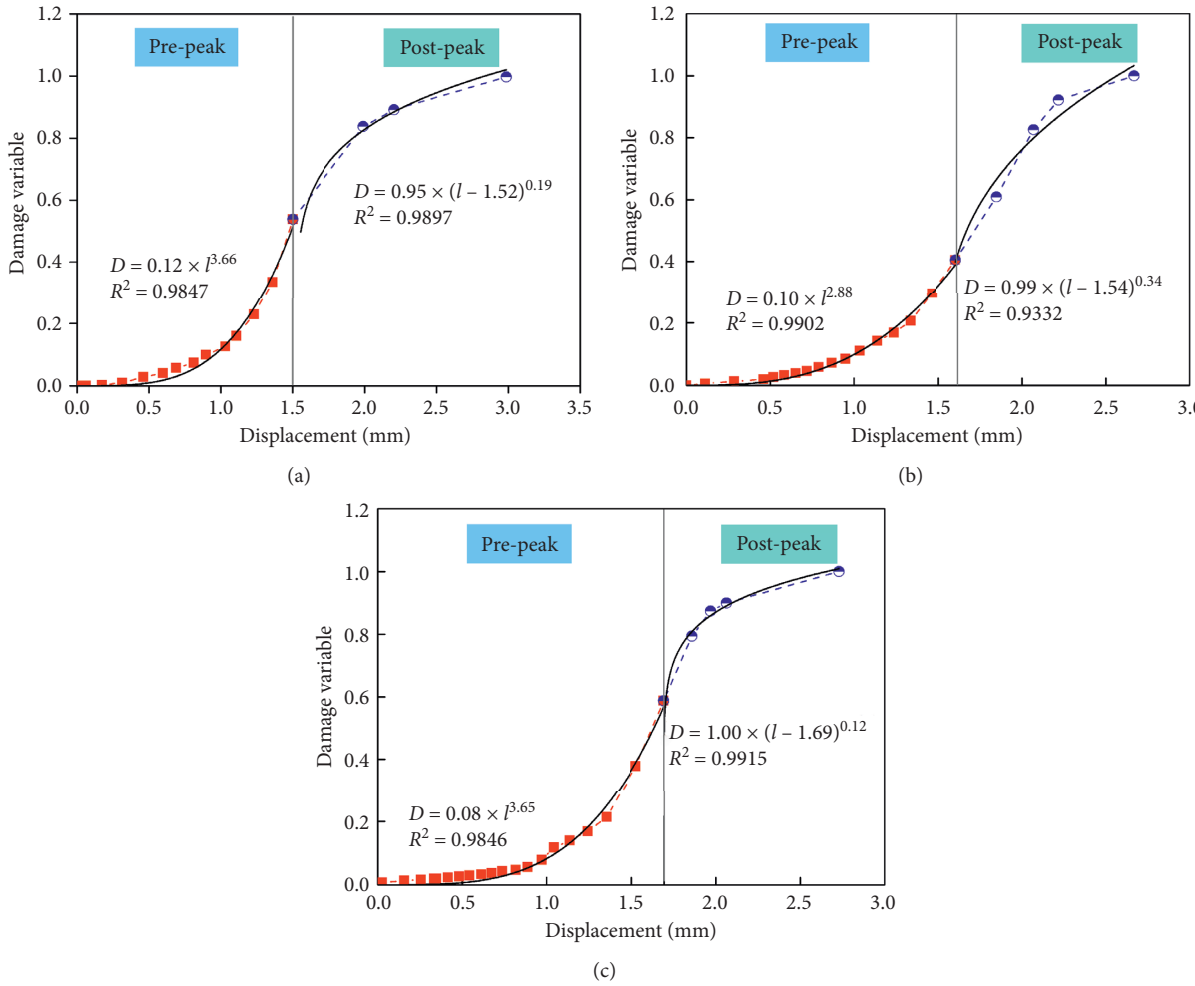


Figure 9: Fitting results of damage variable-displacement curves. (a) Specimen f-1; (b) specimen f-2; (c) specimen f-3.

## 5. Conclusion

In this paper, the changes in the tensile strengths and deformation capacity of salt rock under different loading paths were studied based on uniaxial monotonic loading tension and cyclic tension tests. We also discussed the energy dissipation and damage evolution characteristics of salt rock under uniaxial cyclic tension. The main conclusions are described as follows:

(1) Compared to monotonic tension, both tensile strength and deformation capacity of salt rock are enhanced under cyclic tension. Salt rock is extremely weak under tensile stress as the average tensile strengths of salt rock are 1.07 MPa for monotonic loading and 1.19 MPa for cyclic tension, respectively. The average axial displacement for monotonic loading is 0.81 mm, while the figure for cyclic tension increases by 97.63%.

(2) The variations of proportions of elastic and dissipative energy reflect the damage evolution characteristics of salt rock under cyclic tension. The proportion of dissipative energy $U_d$ is relatively low in elastic stage, and a significant increase happens when entering yield stage. In the yield stage, more elastic energy $U_e$ is stored in the salt rock under low stress but it decreases with the increase in stress, making it approximately a $U$-shape curve. The proportion of dissipative energy rises rapidly in the post-peak stage, indicating that salt rock is greatly damaged after peak stress.

(3) The relationship between damage variable and displacement of salt rock under cyclic tension was established. The damage variable-displacement curves can be divided into two sections, taking the peak stress point as the boundary, and the fitting results show that the relationships between damage variable and displacement can be expressed as power function with different parameters in different stages.

## Data Availability

The data used to support the findings of this study are included within the article.

## Conflicts of Interest

The authors declare that they have no conflicts of interest.

## Acknowledgments

The authors thank the National Natural Science Foundation of China (Grant no. 51874202) and National Ten Thousand Talent Program for financial help.

## References

[1] Z. Hou and K.-H. Lux, "A new coupling concept for the hydro-mechanical interaction of clay stone and rock salt in underground waste repositories," *International Journal of Rock Mechanics and Mining Sciences*, vol. 41, pp. 708–713, 2004.

[2] Q. Zhang, J. Liu, L. Wang et al., "Impurity effects on the mechanical properties and permeability characteristics of salt rock," *Energies*, vol. 13, no. 6, p. 1366, 2020.

[3] E. Wang, K. Khaledi, S. Miro, D. König, and T. Schanz, "Probabilistic analysis of a rock salt cavern with application to energy storage systems," *Rock Mechanics and Rock Engineering*, vol. 50, no. 1, pp. 139–157, 2017.

[4] P. Bérest, B. Brouard, H. Djakeun-Djizanne, and G. Hévin, "Thermomechanical effects of a rapid depressurization in a gas cavern," *Acta Geotechnica*, vol. 9, no. 1, pp. 181–186, 2014.

[5] D. Han, K. Li, and J. Meng, "Evolution of nonlinear elasticity and crack damage of rock joint under cyclic tension," *International Journal of Rock Mechanics and Mining Sciences*, vol. 128, p. 104286, 2020.

[6] L. A. Roberts, S. A. Buchholz, K. D. Mellegard, and U. Düsterloh, "Cyclic loading effects on the creep and dilation of salt rock," *Rock Mechanics and Rock Engineering*, vol. 48, no. 6, pp. 2581–2590, 2015.

[7] L.-J. Ma, X.-Y. Liu, M.-Y. Wang et al., "Experimental investigation of the mechanical properties of rock salt under triaxial cyclic loading," *International Journal of Rock Mechanics and Mining Sciences*, vol. 62, pp. 34–41, 2013.

[8] H. W. Zhou, C. P. Wang, L. Mishnaevsky, Z. Q. Duan, and J. Y. Ding, "A fractional derivative approach to full creep regions in salt rock," *Mechanics of Time-Dependent Materials*, vol. 17, no. 3, pp. 413–425, 2013.

[9] S. R. Taheri, A. Pak, S. Shad, B. Mehrgini, and M. Razifar, "Investigation of rock salt layer creep and its effects on casing collapse," *International Journal of Mining Science and Technology*, vol. 30, no. 3, pp. 357–365, 2020.

[10] H. Mansouri and R. Ajalloeian, "Mechanical behavior of salt rock under uniaxial compression and creep tests," *International Journal of Rock Mechanics and Mining Sciences*, vol. 17, pp. 413–425, 2013.

[11] J. Liu, H. Xie, Z. Hou, C. Yang, and L. Chen, "Damage evolution of rock salt under cyclic loading in unixial tests," *Acta Geotechnica*, vol. 9, no. 1, pp. 153–160, 2014.

[12] S. Wisetsaen, C. Walsri, and K. Fuenkajorn, "Effects of loading rate and temperature on tensile strength and deformation of rock salt," *International Journal of Rock Mechanics and Mining Sciences*, vol. 73, pp. 10–14, 2015.

[13] M. Gerd, "Application of the cluster analysis and time statistic of acoustic emission events from tensile test of a cylindrical rock salt specimen," *Engineering Fracture Mechanics*, vol. 210, pp. 84–94, 2018.

[14] S. M. J. Razavi, M. R. M. Aliha, and F. Berto, "Application of an average strain energy density criterion to obtain the mixed mode fracture load of granite rock tested with the cracked asymmetric four-point bend specimens," *Theoretical and Applied Fracture Mechanics*, vol. 97, pp. 419–425, 2018.

[15] S. Akdag, M. Karakus, G. D. Nguyen, and A. Taheri, "Strain burst vulnerability criterion based on energy-release rate," *Engineering Fracture Mechanics*, vol. 237, p. 107232, 2020.

[16] Y. Deng, M. Chen, Y. Jin, and D. Zou, "Theoretical analysis and experimental research on the energy dissipation of rock crushing based on fractal theory," *Journal of Natural Gas Science and Engineering*, vol. 33, pp. 231–239, 2016.

[17] H. Xie, R. Peng, and Y. Ju, "Energy dissipation of rock deformation and fracture," *Chinese Journal of Rock Mechanics and Engineering*, vol. 23, no. 21, pp. 3565–3570, 2004.

[18] D. Daudon, P. Villard, V. Richefeu, and G. Mollon, "Influence of the morphology of slope and blocks on the energy dissipations in a rock avalanche," *Comptes Rendus Mécanique*, vol. 343, no. 2, pp. 166–177, 2015.

[19] M. Naderloo, M. Moosavi, and M. Ahmadi, "Using acoustic emission technique to monitor damage progress around joints in brittle materials," *Theoretical and Applied Fracture Mechanics*, vol. 104, p. 102368, 2019.

[20] Z. Agioutantis, K. Kaklis, S. Mavrigiannakis, M. Verigakis, F. Vallianatos, and V. Saltas, "Potential of acoustic emissions from three point bending tests as rock failure precursors," *International Journal of Mining Science and Technology*, vol. 26, no. 1, pp. 155–160, 2016.

[21] E. Aker, D. Kühn, V. Vavryčuk, M. Soldal, and V. Oye, "Experimental investigation of acoustic emissions and their moment tensors in rock during failure," *International Journal of Rock Mechanics and Mining Sciences*, vol. 70, pp. 286–295, 2014.

[22] D. Codeglia, N. Dixon, G. J. Fowmes, and G. Marcato, "Analysis of acoustic emission patterns for monitoring of rock slope deformation mechanisms," *Engineering Geology*, vol. 219, pp. 21–31, 2017.

[23] Q. Zhang, J. Liu, H. Xu, Y. Zeng, C. Wang, and L. Wang, "Experimental investigation on permeability evolution of limestone caprock under coupled THM processes," *KSCE Journal of Civil Engineering*, vol. 23, no. 12, pp. 5090–5097, 2019.

[24] (GB/T50266-2013), *National Standards Compilation Group of People's Republic of China. Standard for Tests Method of Engineering Rock Masses*, China Plan Press, Beijing, China, 2013.

[25] M. You and M. Su, "Experimental study on strengthening of amrble specimen in cyclic loading of uniaxial or pseudo-triaxial compression," *Chinese Journal of Solid Mechanics*, vol. 29, no. 1, pp. 66–72, 2008.

[26] J. Zhao, G. Guo, D. Xu et al., "Experimental study of deformation and failure characteristics of deeplu-buried hard rock under triaxial and cyclic stress paths," *Rock and Soil Mechanics*, vol. 41, pp. 1521–1530, 2020.

[27] C. A. Tang and X. H. Xu, "Evolution and propagation of material defects and Kaiser effect function," *Journal of Seismology Research*, vol. 13, no. 2, pp. 203–213, 1990.

[28] B. Q. Li, B. Gonçalves Da Silva, and H. Einstein, "Laboratory hydraulic fracturing of granite: acoustic emission observations and interpretation," *Engineering Fracture Mechanics*, vol. 209, pp. 200–220, 2019.